Seismic Mitigation of Structures Using Direction-Optimized Friction Pendulum System

C. S. Tsai[1], Wen-Shin Chen[2], T. C. Chiang[3], Chen-Tsung Yang[4], Yung-Chang Lin[5]

[1] *Professor, Department of Civil Engineering, Feng Chia University, Taichung, Chinese Taiwan.*
[2] *Ph. D., Graduate Institute of Civil and Hydraulic Engineering, Feng Chia University, Chinese Taiwan.*
[3] *Technical Manage, Earthquake Proof Systems, Taichung, Chinese Taiwan.*
[4] *Master, Department of Civil Engineering, Feng Chia University, Taichung, Chinese Taiwan*
[5] *Ph. D. Candidate, Graduate Institute of Civil and Hydraulic Engineering, Feng Chia University, Taichung, Chinese Taiwan.*
Email: cstsai@fcu.edu.tw

ABSTRACT:

To enhance the capability of structures in seismic mitigation, in this study an advanced base isolation system called the direction optimized-friction pendulum system (DO-FPS) is proposed and investigated to address its mechanical behavior through finite element formulation and examine its efficiency in seismic mitigation by conducting a series of shaking table tests. Based on finite element formulation, it is revealed that the natural period, the capacity of the bearing displacement and damping effect for a Direction Optimized-Friction Pendulum System (DO-FPS) change continually during earthquakes. Therefore, DO-FPS can avoid possibility of resonance of enriched frequencies from ground motions and provide an effective capacity of bearing displacement and damping during the earthquakes. Simultaneously, results from the shaking table tests also illustrate that the DO-FPS isolator possesses an outstanding seismic mitigation capabilities.

KEYWORDS: Earthquake Engineering, Base Isolation, Passive Control, Friction Pendulum System, Base Isolator

1. INTRODUCTION

In recent years, there are more and more seismic engineering applications of the base isolation technology for upgrading the seismic resistibility of their superstructures. Either from experimental results or earthquake experiences, base isolation has been proven as a good tool for enhancing the seismic resistibility of existing structures and new construction structures. A new base isolator called the Directional Optimization Friction Pendulum System (DO-FPS), Figure 1, will be proposed in this study. The structure of the new device is composed of a spherical sliding surface, a concave trench sliding surface and an articulated slider. Based on this special design, the isolation period is dependent on the angle between the resultant displacement and the fixed local coordinate system. Hence, the resonance of the base isolated structure which may result in the failure of the base isolator under severe earthquakes will be prevented. In order to verify the mechanical characteristics of the proposed device, the finite element formulations will be presented in this study. It is shown from the formulations that the isolation period is indeed dependent on the angle between the resultant displacement and the fixed local coordinate system. As the resultant sliding displacement parallels the direction of the trench, the DO-FPS behaves as the Multiple Friction Pendulum System [1,2]. However, the behavior of the proposed device is the same as that of the Friction Pendulum System [3] whenever the resultant displacement and the direction of the trench are perpendicular with each other. To verify the efficiency of the proposed isolator, the shaking table tests of a three story steel structure with DO-FPS isolators have been performed. The experimental results from shaking table tests show that the acceleration responses of the base isolated structure are much smaller than those of the fixed base structure. Therefore, the new device proposed in this study can be recognized as a reliable and cost-effective device in seismic engineering.

2. FINITE ELEMENT FORMULATIONS FOR DO-FPS

In order to simulate the nonlinear behavior of the DO-FPS isolator, as shown in Figure 2, a two-node finite

element is proposed in this study. As shown in Figures 3 and 4, this two-node finite element includes one node each at the center of the spherical concave surface (node 1) and trench concave (node 2) surfaces. As shown in Figure 3, the equilibrium of the spherical concave surface in the horizontal and vertical directions can be expressed as following [4-7]:

$$F_1 - P_1\sin\theta_1 - T_1\cos\theta_1 = 0 \tag{1}$$

$$W - P_1\cos\theta_1 + T_1\sin\theta_1 = 0 \tag{2}$$

where W is the vertical load resulting from the superstructure including the static and seismic loads; P_1, the contact force normal to the spherical concave surface; T_1, the tangential component of the frictional force in the F-W plane; F_1, the horizontal force imposed on the spherical concave surface; and θ_1, the rotational angle between the articulated slider and the center of the spherical surface.

Rearrangement of eq. (2) gives

$$P_1 = \frac{W + T_1\sin\theta_1}{\cos\theta_1} \tag{3}$$

The back-substitution of eq. (3) into eq. (1) leads to

$$F_1 = W\tan\theta_1 + \frac{T_1}{\cos\theta_1} = \bar{k}_{r1}\bar{D}_{r1} + \frac{T_1}{\cos\theta_1} \tag{4}$$

where

$$\bar{k}_{r1} = \frac{W}{R_1\cos\theta_1} \tag{5}$$

$$\bar{D}_{r1} = R_1\sin\theta_1 \tag{6}$$

In which $\bar{k}_{r1}$ is the horizontal stiffness of the spherical concave surface; $\bar{D}_{r1}$, the sliding displacement of the articulated slider relative to the center of the spherical concave surface; And R_1, the radius of curvature of the spherical concave surface.

As shown in Figure 5, the horizontal force F_1 in the F-W plane of the spherical concave surface can be transformed into the local coordinate system as follows:

$$\bar{F}_2 = F_1\cos\alpha = \bar{k}_{r1}\bar{D}_{r1}\cos\alpha + \frac{T_1}{\cos\theta_1}\cos\alpha \tag{7}$$

Where $\bar{F}_2$ is the horizontal force in the ς direction.

As shown in Figure 3, the horizontal displacement $\bar{D}_{r1}$ can be expressed as:

$$\bar{D}_{r1} = \bar{u}_2^*\cos\alpha + \bar{u}_3^*\sin\alpha \tag{8}$$

where $\bar{u}_2^*$ and $\bar{u}_3^*$ represent the horizontal displacements of the spherical concave surface relative to the articulated slider in the ς and η directions, respectively.

The back-substitution of eq. (8) into eq. (7) leads to

$$\bar{F}_2 = (\bar{k}_{r1}\cos^2\alpha)\bar{u}_2^* + (\bar{k}_{r1}\sin\alpha\cdot\cos\alpha)\bar{u}_3^* + \frac{T_1}{\cos\theta_1}\cos\alpha \tag{9}$$

Similarly, the horizontal force $\bar{F}_3$ in the η direction is

$$\bar{F}_3 = (\bar{k}_{r1}\sin\alpha\cdot\cos\alpha)\cdot\bar{u}_2^* + (\bar{k}_{r1}\sin^2\alpha)\bar{u}_3^* + \frac{T_1}{\cos\theta_1}\sin\alpha \tag{10}$$

As shown in Figures 6 and 7, the equilibrium of the trench concave surface in the ς and η directions are:

$$\bar{F}_2 - P_2\sin\theta_2 - T_2\cos\theta_2 - \mu_s\left|\bar{F}_3\right|\mathrm{sgn}(\dot{\bar{u}}_2^{**}) = 0 \tag{11}$$

and

$$W - P_2\cos\theta_2 + T_2\sin\theta_2 = 0 \tag{12}$$

where W is the vertical load resulting from the superstructure; P_2, the contact force normal to the trench concave surface; T_2, the tangential component of the frictional force in the F-W plane; $\bar{F}_2$ and $\bar{F}_3$, the

horizontal forces acting on the trench concave surface in the ς and the η directions, respectively; θ_2, the rotational angle between the articulated slider and the center of the trench concave surface; $\dot{\bar{u}}_2^{**}$ is the relative velocity in the ς direction between the articulated slider and the trench concave sliding surface and μ_s, the frictional coefficient provided by the wall of the trench concave surface.

The rearrangement of eqs. (11) and (12) yields:

$$\bar{F}_2 = W\tan\theta_2 + \frac{T_2}{\cos\theta_2} + \mu_s\left|\bar{F}_3\right|\mathrm{sgn}(\dot{\bar{u}}_2^{**}) = \bar{k}_{r2}\bar{u}_2^{**} + \frac{T_2}{\cos\theta_2} + \mu_s\left|\bar{F}_3\right|\mathrm{sgn}(\dot{\bar{u}}_2^{**}) \tag{13}$$

where

$$\bar{k}_{r2} = \frac{W}{R_2\cos\theta_2} \tag{14}$$

$$\bar{u}_2^{**} = R_2\sin\theta_2 \tag{15}$$

$\bar{k}_{r2}$ is the horizontal stiffness of the trench concave surface; $\bar{u}_2^{**}$ is the relative displacement in the ς direction between the articulated slider and the trench concave sliding surface and R_2, the radius of the trench concave surface.

Because the horizontal stiffness in the η direction of the trench concave surface is relatively high, parameter E_∞ can be adopted in the following equation:

$$\bar{F}_3 = E_\infty\bar{u}_3^{**} \tag{16}$$

where $\bar{u}_3^{**}$ denotes the relative horizontal displacement between node 2 and the articulated slider in the η direction. In addition, there is no relative horizontal displacement of the trench concave surface to the articulated slider along the η direction. Thus, the rearrangement of eq. (16) results in

$$\bar{u}_3^{**} = \frac{\bar{F}_3}{E_\infty} = 0 \tag{17}$$

According to eqs. (9) and (13), the horizontal displacements of the spherical and trench sliding surfaces in the ς direction can be respectively expressed as

$$\bar{u}_2^{*} = [\bar{F}_2 - (\bar{k}_{r1}\sin\alpha\cdot\cos\alpha)\cdot\bar{u}_3^{*} - \frac{T_1}{\cos\theta_1}\cos\alpha]\Big/\bar{k}_{r1}\cos^2\alpha \tag{18}$$

and

$$\bar{u}_2^{**} = [\bar{F}_2 - \frac{T_2}{\cos\theta_2} - \mu_s\left|\bar{F}_3\right|\mathrm{sgn}(\dot{\bar{u}}_2^{**})]\Big/\bar{k}_{r2} \tag{19}$$

Therefore, the total sliding displacement of the base isolator in the ς direction can be given as

$$\bar{u}_2 = \bar{u}_2^{*} + \bar{u}_2^{**} = \frac{\bar{k}_{r2}\left[\bar{F}_2 - (\bar{k}_{r1}\sin\alpha\cdot\cos\alpha)\cdot\bar{u}_3^{*} - \frac{T_1}{\cos\theta_1}\cos\alpha\right] + \bar{k}_{r1}\cos^2\alpha\left[\bar{F}_2 - \frac{T_2}{\cos\theta_2} - \mu_s\left|\bar{F}_3\right|\mathrm{sgn}(\dot{\bar{u}}_2^{**})\right]}{\bar{k}_{r1}\bar{k}_{r2}\cos^2\alpha} \tag{20}$$

The shear force in the ς direction expressed in eq. (21) can be gained by rearranging eq. (20) as follows:

$$\bar{F}_2 = \frac{\bar{k}_{r1}\bar{k}_{r2}\cos^2\alpha}{\bar{k}_{r1}\cos^2\alpha + \bar{k}_{r2}}\bar{u}_2 + \frac{\bar{k}_{r1}\bar{k}_{r2}\sin\alpha\cdot\cos\alpha}{\bar{k}_{r1}\cos^2\alpha + \bar{k}_{r2}}\bar{u}_3^{*} + \frac{1}{\bar{k}_{r1}\cos^2\alpha + \bar{k}_{r2}}\left[\bar{k}_{r2}\frac{T_1}{\cos\theta_1}\cos\alpha + \bar{k}_{r1}\frac{T_2}{\cos\theta_2}\cos^2\alpha + \bar{k}_{r1}\mu_s\left|\bar{F}_3\right|\mathrm{sgn}(\dot{\bar{u}}_2^{**})\cos^2\alpha\right] \tag{21}$$

Similarly, on rearranging eq. (10), the relative horizontal displacement of the lower spherical concave surface to the articulated slider in the η direction can be shown as

$$\bar{u}_3^{*} = [\bar{F}_3 - (\bar{k}_{r1}\sin\alpha\cdot\cos\alpha)\cdot\bar{u}_2^{*} - \frac{T_1}{\cos\theta_1}\sin\alpha]\Big/\bar{k}_{r1}\sin^2\alpha \tag{22}$$

In addition, according to eqs. (17) and (22), the total horizontal displacement of the DO-FPS isolator in the η direction can be obtained as

$$\bar{u}_3 = \bar{u}_3^* + \bar{u}_3^{**} = \bar{u}_3^{**} = [\bar{F}_3 - \left(\bar{k}_{r1}\sin\alpha\cdot\cos\alpha\right)\cdot\bar{u}_2^* - \frac{T_1}{\cos\theta_1}\sin\alpha]\Big/\bar{k}_{r1}\sin^2\alpha \tag{23}$$

Simultaneously, the shear force in the η direction can be shown as

$$\bar{F}_3 = \bar{k}_{r1}\sin\alpha\cdot\cos\alpha\,\bar{u}_2^* + \bar{k}_{r1}\sin^2\alpha\,\bar{u}_3 + \frac{T_1}{\cos\theta_1}\sin\alpha \tag{24}$$

Subsequently eq. (21) can be rewritten as

$$\begin{aligned}\bar{F}_2 = {} & \frac{\bar{k}_{r1}\bar{k}_{r2}\cos^2\alpha}{\bar{k}_{r1}\cos^2\alpha+\bar{k}_{r2}}\bar{u}_2 + \frac{\bar{k}_{r1}\bar{k}_{r2}\sin\alpha\cdot\cos\alpha}{\bar{k}_{r1}\cos^2\alpha+\bar{k}_{r2}}\bar{u}_3 \\ & + \frac{1}{\bar{k}_{r1}\cos^2\alpha+\bar{k}_{r2}}\left[\bar{k}_{r2}\frac{T_1}{\cos\theta_1}\cos\alpha + \bar{k}_{r1}\frac{T_2}{\cos\theta_2}\cos^2\alpha + \bar{k}_{r1}\mu_s\left|\bar{F}_3\right|\mathrm{sgn}(\dot{\bar{u}}_2^{**})\cos^2\alpha\right]\end{aligned} \tag{25}$$

Simultaneously, the back-substitution of eq. (25) into eq. (18) then the subsequent back-substitution of eq. (18) into eq. (24) and finally the rearrangement of eq. (24) leads to

$$\begin{aligned}\bar{F}_3 = {} & \frac{\bar{k}_{r1}\bar{k}_{r2}\sin\alpha\cdot\cos\alpha}{\bar{k}_{r1}\cos^2\alpha+\bar{k}_{r2}}\bar{u}_2 + \frac{\bar{k}_{r1}\bar{k}_{r2}\sin^2\alpha}{\bar{k}_{r1}\cos^2\alpha+\bar{k}_{r2}}\bar{u}_3 \\ & + \frac{1}{\bar{k}_{r1}\cos^2\alpha+\bar{k}_{r2}}\left[\bar{k}_{r2}\frac{T_1}{\cos\theta_1}\sin\alpha + \bar{k}_{r1}\frac{T_2}{\cos\theta_2}\sin\alpha\cos\alpha + \bar{k}_{r1}\mu_s\left|\bar{F}_3\right|\mathrm{sgn}(\dot{\bar{u}}_2^{**})\sin\alpha\cos\alpha\right]\end{aligned} \tag{26}$$

Because the vertical stiffness of the base isolator is relatively high, a large stiffness can be used in the numerical simulation:

$$\bar{F}_1 = E_\infty\bar{u}_1 \tag{27}$$

Rearranging eqs. (25), (26), and (27) can lead to

$$\begin{bmatrix}\bar{F}_1\\ \bar{F}_2\\ \bar{F}_3\end{bmatrix} = \begin{bmatrix}E_\infty & 0 & 0\\ 0 & \frac{\bar{k}_{r1}\bar{k}_{r2}\cos^2\alpha}{\bar{k}_{r1}\cos^2\alpha+\bar{k}_{r2}} & \frac{\bar{k}_{r1}\bar{k}_{r2}\sin\alpha\cdot\cos\alpha}{\bar{k}_{r1}\cos^2\alpha+\bar{k}_{r2}}\\ 0 & \frac{\bar{k}_{r1}\bar{k}_{r2}\sin\alpha\cdot\cos\alpha}{\bar{k}_{r1}\cos^2\alpha+\bar{k}_{r2}} & \frac{\bar{k}_{r1}\bar{k}_{r2}\sin^2\alpha}{\bar{k}_{r1}\cos^2\alpha+\bar{k}_{r2}}\end{bmatrix}\begin{Bmatrix}\bar{u}_1\\ \bar{u}_2\\ \bar{u}_3\end{Bmatrix} + \begin{Bmatrix}0\\ \frac{1}{\bar{k}_{r1}\cos^2\alpha+\bar{k}_{r2}}\left[\bar{k}_{r2}\frac{T_1}{\cos\theta_1}\cos\alpha + \bar{k}_{r1}\frac{T_2}{\cos\theta_2}\cos^2\alpha + \bar{k}_{r1}\mu_s\left|\bar{F}_3\right|\mathrm{sgn}(\dot{\bar{u}}_2^{**})\cos^2\alpha\right]\\ \frac{1}{\bar{k}_{r1}\cos^2\alpha+\bar{k}_{r2}}\left[\bar{k}_{r2}\frac{T_1}{\cos\theta_1}\sin\alpha + \bar{k}_{r1}\frac{T_2}{\cos\theta_2}\sin\alpha\cdot\cos\alpha + \bar{k}_{r1}\mu_s\left|\bar{F}_3\right|\mathrm{sgn}(\dot{\bar{u}}_2^{**})\sin\alpha\cdot\cos\alpha\right]\end{Bmatrix} \tag{28}$$

As shown in Figure 7, the friction force Q_1 acting in the lower concave surface should be taken into account:

$$\begin{aligned}\begin{bmatrix}\bar{F}_1\\ \bar{F}_2\\ \bar{F}_3\end{bmatrix} = {} & \begin{bmatrix}E_\infty & 0 & 0\\ 0 & \frac{\bar{k}_{r1}\bar{k}_{r2}\cos^2\alpha}{\bar{k}_{r1}\cos^2\alpha+\bar{k}_{r2}} & \frac{\bar{k}_{r1}\bar{k}_{r2}\sin\alpha\cdot\cos\alpha}{\bar{k}_{r1}\cos^2\alpha+\bar{k}_{r2}}\\ 0 & \frac{\bar{k}_{r1}\bar{k}_{r2}\sin\alpha\cdot\cos\alpha}{\bar{k}_{r1}\cos^2\alpha+\bar{k}_{r2}} & \frac{\bar{k}_{r1}\bar{k}_{r2}\sin^2\alpha}{\bar{k}_{r1}\cos^2\alpha+\bar{k}_{r2}}\end{bmatrix}\begin{Bmatrix}\bar{u}_1\\ \bar{u}_2\\ \bar{u}_3\end{Bmatrix} + \begin{Bmatrix}0\\ \frac{1}{\bar{k}_{r1}\cos^2\alpha+\bar{k}_{r2}}\left[\bar{k}_{r2}\frac{T_1}{\cos\theta_1}\cos\alpha + \bar{k}_{r1}\frac{T_2}{\cos\theta_2}\cos^2\alpha + \bar{k}_{r1}\mu_s\left|\bar{F}_3\right|\mathrm{sgn}(\dot{\bar{u}}_2^{**})\cos^2\alpha\right] + Q_1\sin\alpha\\ \frac{1}{\bar{k}_{r1}\cos^2\alpha+\bar{k}_{r2}}\left[\bar{k}_{r2}\frac{T_1}{\cos\theta_1}\sin\alpha + \bar{k}_{r1}\frac{T_2}{\cos\theta_2}\sin\alpha\cdot\cos\alpha + \bar{k}_{r1}\mu_s\left|\bar{F}_3\right|\mathrm{sgn}(\dot{\bar{u}}_2^{**})\sin\alpha\cdot\cos\alpha\right] - Q_1\cos\alpha\end{Bmatrix}\\ = {} & \bar{\mathbf{K}}\mathbf{U}(t) + \mathbf{S}(t)\end{aligned} \tag{29}$$

The natural frequency of the DO-FPS isolator can be obtained as:

$$\omega^2 = \frac{1}{m}\left(\frac{\bar{k}_{r1}\bar{k}_{r2}}{\bar{k}_{r1}\cos^2\alpha+\bar{k}_{r2}}\right) = \frac{g}{R_1\cos\theta_1 + R_2\cos\theta_2\cos^2\alpha} \tag{30}$$

where m is the mass acting on the base isolator. If the angles θ_1 and θ_2 are small, then $\cos\theta_1 \approx \cos\theta_2 \approx 1$, and eq. (30) can be rewritten as:

$$\omega = \sqrt{\frac{g}{R_1 + R_2 \cos^2 \alpha}} \tag{31}$$

The displacement capacity of the DO-FPS isolator, D_c, is also a function of the angle α and given as:

$$D_c = \pm(R_{sc} + R_{tc}\cos\alpha - D_s) \tag{32}$$

where R_{sc} is the radius of the spherical concave surface in the horizontal plane, R_{tc} is the half length of the trench concave surface in the horizontal plane; and D_s is the radius of the slider.

If $\alpha = 0^\circ$, the natural frequency of the DO-FPS isolator is given by:

$$\omega = \sqrt{\frac{g}{R_1 + R_2}} \tag{33}$$

Similarly, if $\alpha = 90^\circ$, the natural frequency is identical to FPS:

$$\omega = \sqrt{\frac{g}{R_1}} \tag{34}$$

In addition, if the angles θ_1 and θ_2 are small, the equivalent damping is defined as the following equation [16]:

$$\beta_{eff} = \frac{E_D}{4\pi E_S} = \frac{2}{\pi}\left[\frac{R_1\mu_1 + R_2\mu_2 \cos\alpha}{(\bar{u}_2 \cos\alpha + \bar{u}_3 \sin\alpha) + (R_1\mu_1 + R_2\mu_2 \cos\alpha)}\right] \tag{35}$$

where E_D is the energy dissipated by the DO-FPS isolator; E_S is the elastic strain energy of the DO-FPS isolator; μ_1 and μ_2 indicate the friction coefficients of the spherical concave surface and the trench concave surface, respectively.

3. SHAKING TABLE TESTS OF A THREE STORY STEEL STRUCTURE

In order to understand the efficiency of the proposed isolator, a series of shaking table tests of a three story steel structure isolated with DO-FPS were performed in the Department of Civil Engineering, Feng Chia University, Taichung, Taiwan. The sizes of three story steel structure are 1.1m×1.1m in plane and 2.7m in tall. In order to simulate loadings on floor, we put 400kg masses at each floor. The total mass including the mass of the structure is about 2.0 tons as shown in Fig. 8. In this study, we used 0.5g accelerations of the El Centro earthquake (U.S.A., 1940) and Chi-Chi earthquake (Taiwan, 1999) for vibration simulations to understand the seismic responses of structure with DO-FPS while $\alpha = 0$ and $\alpha = 90$. Figs.9 to 10 display time history responses of roof accelerations of the structure with and without DO-FPS isolators under various earthquakes. It is illustrated that the proposed isolator can effectively reduce accelerations under various earthquakes. Its efficiencies are shown in Tables 1 and 2. From the shaking table tests of the three story steel structure equipped with proposed isolators, it is demonstrated that the DO-FPS isolator is a promising device which can reduce the seismic responses of the superstructure.

4. CONCLUSIONS

A new base isolator with variable isolation periods in different directions has been proposed in this study. The mathematical model of the DOFPS presented in this study shows that the fundamental period is dependent on the angle between the resultant sliding displacement and the fixed local coordinate system. Therefore, the DOFPS can prevent resonance. It is shown from the results of the shaking table tests that the base isolator can reduce the seismic responses of the superstructure in the range of 70~80%. Therefore, the proposed device can be recognized as an excellent tool for upgrading the seismic resistibility of the traditional fixed base structure during severe earthquakes.

REFERENCES

[1] Tsai, C. S., Chen W.S., Chiang T.C. and Chen B. J. (2006). Component and Shaking Table Tests for Full-Scale Multiple Friction Pendulum System. *Earthquake Engineering and Structural Dynamics*, **35**, 1653-1675.

[2] Fenz,D. M., Constantinou, M. C. (2006), "Behaviour of the Doubled Concave Friction Pendulum System", Earthquake Engineering and Structural Dynamics, Vol. 35, pp.1403-1424.

[3] Zayas,V. A., Low, S. S. and Mahin, S. A. (1987).The FPS Earthquake Resistiing System Experimental Report. Technical Report, UBC/EERC-87/01.

[4] Tsopelas P, Constantinou M.C., Kim Y.S., Okamoto S. Experimental study of FPS system in bridge seismic isolation. *Earthquake Engineering and Structural Dynamics*, 1996; **25**: 65-78.

[5] Tsai C.S., Chiang T.C., Chen W.S., Yang C.T. and Lin J.L. Finite Element Formulations and Experimental Study for Direction Optimized-Friction Pendulum System. *Seismic Engineering 2007, ASME*, Edited by Tom Clark, San Antonio, Texas, U.S.A., July 22-26, 2007; NO. PVP2007-26521.

[6] Tsai C.S., Chen W.S., Chiang T.C. and Lin Y.C. Application of Direction Optimized-Friction Pendulum System to Seismic Mitigation of Sensitive Equipment. *Seismic Engineering 2007, ASME*, Edited by Tom Clark, San Antonio, Texas, U.S.A., July 22-26, 2007; NO. PVP2007-26552.

[7] Tsai C.S., Chen W.S. and Chiang T.C. Finite Element Formulations for Direction Optimized-Variable Curvature Friction Pendulum System. *Seismic Engineering 2007, ASME*, Edited by Tom Clark, San Antonio, Texas, U.S.A., July 22-26, 2007; NO. PVP2007-26555.

Table 1 Acceleration Efficiency of DOFPS (α=0)

Max. Response	Roof Acceleration(g)			
Earthquake	Amplitude	El Centro	Kobe	Chi-Chi
Bare Structure	0.483g	2.010	1.307	0.963
Isolated Structure	0.483g	0.317	0.268	0.261
Response Reduction	0.483g	84.25%	79.46%	72.88%

Table 2 Acceleration Efficiency of DOFPS (α=90)

Max. Response	Roof Acceleration(g)			
Earthquake	Amplitude	El Centro	Kobe	Chi-Chi
Bare Structure	0.483g	2.018	1.307	0.930
Isolated Structure	0.483g	0.320	0.294	0.382
Response Reduction	0.483g	84.13%	77.51%	58.97%

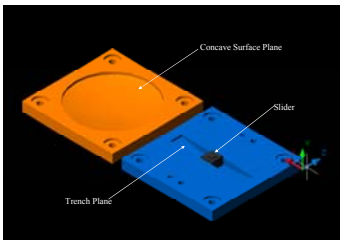

Figure 1 Directional Optimizated Friction Pendulum System

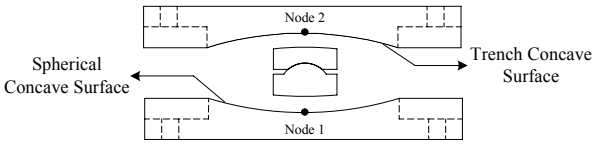

Figure 2 Two-node element of the DO-FPS isolator

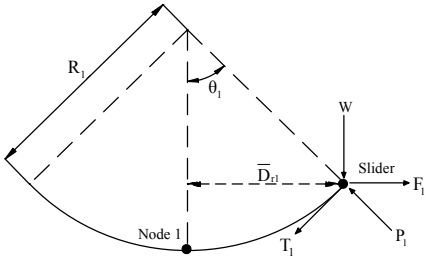

Figure 3 Equilibrium of the spherical concave Surface in the F-W plane

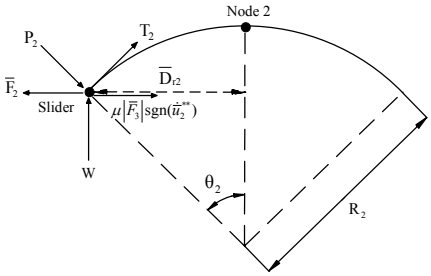

Figure 4 Equilibrium of the trench concave surface

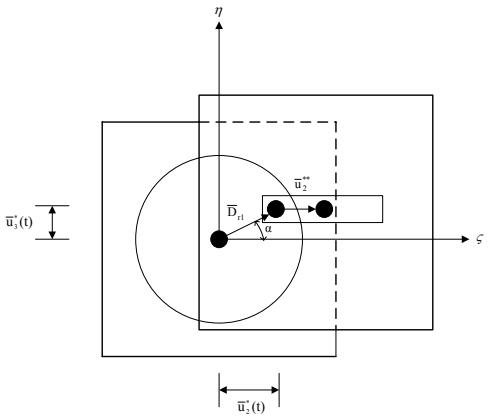

Figure 5 Top view of the motion of the DO-FPS isolator

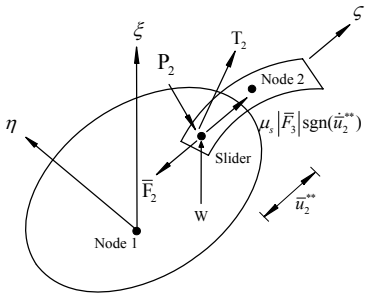

Figure 6 Forces acting on trench concave surface

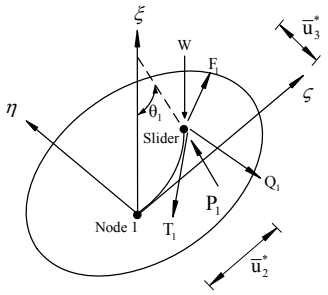

Figure 7 Forces acting on spherical sliding surface

Figure 8 A Three Story Steel Structure

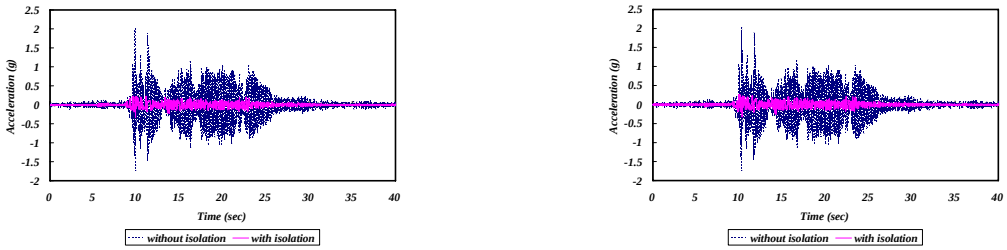

(a) α = 0 **(b)** α = 90

Figure 9 Roof acceleration of structure with and without DO-FPS isolator under El Centro earthquake with 0.483g in PGA

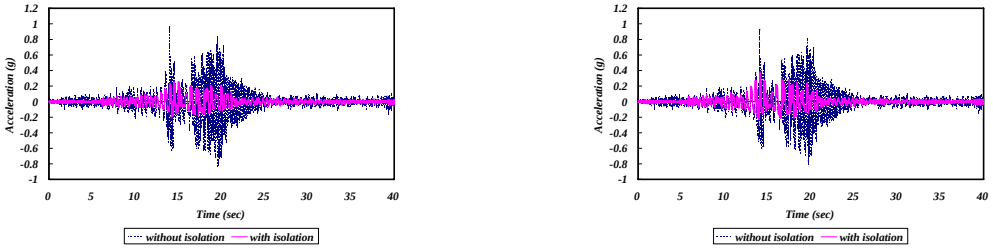

(a) α = 0 **(b)** α = 90

Figure 10 Roof acceleration of structure with and without DO-FPS isolator under Chi-Chi earthquake with 0.483g in PGA